



HAL
open science

Modelling of the Programming Window Distribution in Multi Nanocrystals Memories

Luca Perniola, Barbara De Salvo, Gérard Ghibaudo, Armando Foglio Para, Georges Pananakakis, Vincent Vidal, Thierry Baron, Salvatore Lombardo

► **To cite this version:**

Luca Perniola, Barbara De Salvo, Gérard Ghibaudo, Armando Foglio Para, Georges Pananakakis, et al.. Modelling of the Programming Window Distribution in Multi Nanocrystals Memories. ESSDERC, 2003, Lisbon, Portugal. 10.1109/TNANO.2003.820782 . hal-00485165

HAL Id: hal-00485165

<https://hal.science/hal-00485165v1>

Submitted on 13 Oct 2022

HAL is a multi-disciplinary open access archive for the deposit and dissemination of scientific research documents, whether they are published or not. The documents may come from teaching and research institutions in France or abroad, or from public or private research centers.

L'archive ouverte pluridisciplinaire **HAL**, est destinée au dépôt et à la diffusion de documents scientifiques de niveau recherche, publiés ou non, émanant des établissements d'enseignement et de recherche français ou étrangers, des laboratoires publics ou privés.



Distributed under a Creative Commons Attribution - NonCommercial 4.0 International License

Modeling of the Programming Window Distribution in Multinanocrystals Memories

Luca Perniola, Barbara De Salvo, Gérard Ghibaudo, Armando Foglio Para, G. Pananakakis, V. Vidal, Thierry Baron, and Salvatore A. Lombardo

Abstract—In this paper, the impact of the Si nanocrystals technological fluctuations on the programming window dispersion of multi nanocrystals memory is thoroughly investigated. Technological dispersions of different nanocrystals populations, directly measured by high-resolution transmission electron microscopy, are used as starting points for the modeling of the device characteristics. Numerical Monte Carlo simulations as well as an original compact modeling, based on the compound distributions (CD) statistics, are here presented. Exact analytical results (CD model), approximated analytical results (CD+Central Limit Theorem model) and numerical results (numerical convolution) are deeply discussed. Finally, the good agreement between our simulations and experimental data of ultrascaled nanocrystal devices, made by conventional UV lithography or by e-beam lithography, definitively confirms the validity of our theoretical approach.

Keywords—Compound distributions, multinanocrystal memories, programming window distribution.

I. INTRODUCTION

MULTINANOCRYSTAL memory devices are widely invoked as one of the possible solutions to the scaling limitation of Flash memory devices [1]. In fact, the use of discrete trap storage nodes in flash memories, instead of a continuum floating gate (FG), guarantees insensitivity to stress-induced oxide defects, allowing for thinner tunnel oxides [2]. Moreover, these devices do not suffer of drain turn-on effect [3], allowing for cell length scaling and high reading drain voltage. In conventional FG devices, the intra-die variation of natural threshold voltage, due to dopant fluctuations of the well doping, has been ascribed as a major reliability concern as devices continue to scale [4].

In spite of the previously remembered advantages of nanocrystals devices compared to conventional FG devices, in nanocrystal memories an additional cause of fluctuations of electrical characteristics will exist. In fact, *fluctuations of dot diameter and dot number* from one sample to another will be more and more critical for ultrascaled memory cells containing

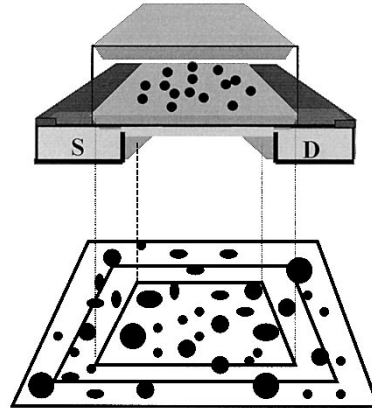


Fig. 1. The multinanocrystals memory device structure. The dot size and dot number fluctuations in memory cell of different areas are illustrated.

a very little number of dots (Fig. 1). In particular, the dispersion of the programming window ($\sigma\Delta V_{th}$) will raise while scaling the cell area. In order to control this new critical issue, a very strict control of dot deposition parameters has to be assured.

The aim of this paper is to quantitatively evaluate the scaling limit of this novel concept of memory based on randomly distributed storage sites. The statistical description of the dots parameter fluctuations and their impacts on device characteristics will be here addressed both from a theoretical and an experimental point of view.

II. TECHNOLOGICAL FLUCTUATIONS OF SILICON NANOCRYSTALS: DOT DIAMETER AND DOT NUMBER

The storing properties of a nanocrystals memory cell depend both on the *total dot number*, N_{td} , and *dot diameter*, Φ , on the cell. Indeed, these two main parameters strictly depend on the process conditions used for Silicon nanocrystals deposition. Today, the low-pressure chemical vapor deposition [1], [5] is one of the most promising fabrication method for integration of nanocrystals technologies in industrial circuits. Based on this approach, the total dot number, N_{td} , and dot diameter, Φ , could be regarded as independent statistical variables as the state-of-the-art low-pressure chemical vapor deposition (LPCVD) knowledge does not allow deposition of a fixed dot number nor an uniquely defined dot size.

A. Maxwell–Boltzmann Fit for Dot Diameter

Concerning the dot diameter Φ , a phenomenological approach is taken. In particular, the probability density is obtained

L. Perniola is with IMEP-CNRS/INPG, Grenoble 38016, France, and also with CEA-LETI, Grenoble 38054, France (e-mail: perniola@enserg.fr).

B. De Salvo and V. Vidal are with CEA-LETI, Grenoble 38054, France.

G. Ghibaudo and G. Pananakakis are with IMEP-CNRS/INPG, Grenoble 38016, France.

A. F. Para is with the Politecnico di Milano, Milano 20133, Italy.

T. Baron is with LTM-CNRS/UJF, Grenoble 38016, France.

S. A. Lombardo is with IMM-CNR, Catania 95121, Italy.

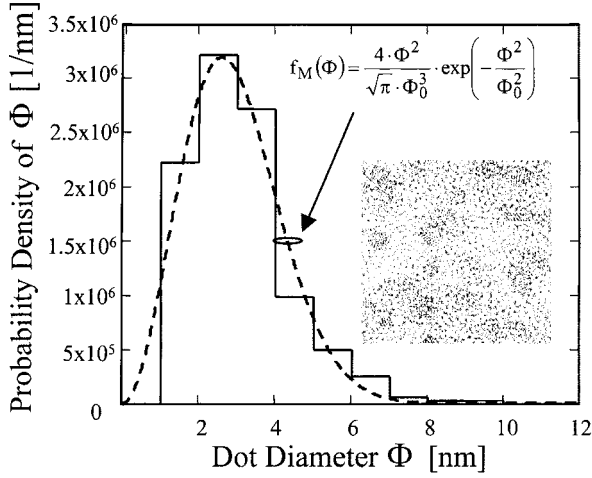


Fig. 2. Dot diameter experimental distribution coming from the TEM image of LPCVD Si-dots (inset, highest dot density ever reached in the literature $D_{\text{dot}} = 2 \times 10^{12} \text{ cm}^{-2}$, mean dot diameter $\sim 3 \text{ nm}$) and theoretical fitting (dashed line) based on a Maxwell-Boltzmann distribution ($\Phi_0 = 2.7 \text{ nm}$ most probable diameter, $\sigma^2 \Phi^2 / \Phi_0^2 = 2/3$).

by directly fitting the experimental dot size histograms (measured by high-resolution transmission electron microscopy) of LPCVD nanocrystals successively integrated in memory devices. Note, that this phenomenological approach is not substantive for the smallest dot diameter values (less than 1 nm), as TEM imaging is not able to devise such small objects.

Two different populations of nanocrystals were considered. Fig. 2 illustrates the statistics of silicon dots with a high areal density, $2 \times 10^{12} \text{ dots/cm}^2$, and a mean diameter of $\sim 3 \text{ nm}$ [5]. Note, that at our knowledge, this is the highest Si-dot density ever obtained by LPCVD technique on SiO_2 substrates. This populations can be fitted by a *Maxwell-Boltzmann distribution*

$$P_M(\Phi, \Phi_0) = \frac{4\Phi^2}{\sqrt{\pi} \cdot \Phi_0^3} \cdot \exp\left(-\frac{\Phi^2}{\Phi_0^2}\right) d\Phi \quad (1)$$

where Φ_0 denotes the most probable dot diameter present in the statistical ensemble.

For the purposes of the following theoretical analysis, it should be highlighted that the Maxwell-Boltzmann distribution is a chi-squared function of three degrees of freedom [6]. Indeed, by putting $x/2 = \Phi^2/\Phi_0^2$, and introducing the identity $2 \cdot \sqrt{\pi} = \Gamma(3/2)$, we see

$$\frac{4\Phi^2}{\sqrt{\pi} \cdot \Phi_0^3} \cdot \exp\left(-\frac{\Phi^2}{\Phi_0^2}\right) \cdot d\Phi = \frac{\sqrt{\frac{x}{2}}}{2 \cdot \Gamma\left(\frac{3}{2}\right)} \cdot \exp\left(-\frac{x}{2}\right) \cdot dx. \quad (2)$$

B. Shneidman Assumption for Dot Diameter

Fig. 3 illustrates the statistics of Silicon dots with a small areal density, $6 \times 10^{11} \text{ dots/cm}^2$, and a mean diameter $\sim 4.9 \text{ nm}$ (in the inset a Energy Filtered TEM image is shown) [3]. For this type of statistics, another theoretical approach is more suitable: the *Shneidman model*, based on the well-known capillarity model [7].

In this, the free energy change due to the formation of a cluster of size i is the balance between the gain of volume free energy $\Delta g_v^* i$ due to condensation of the i atoms in the new phase, and the loss due to surface energies of the new formed interfaces,

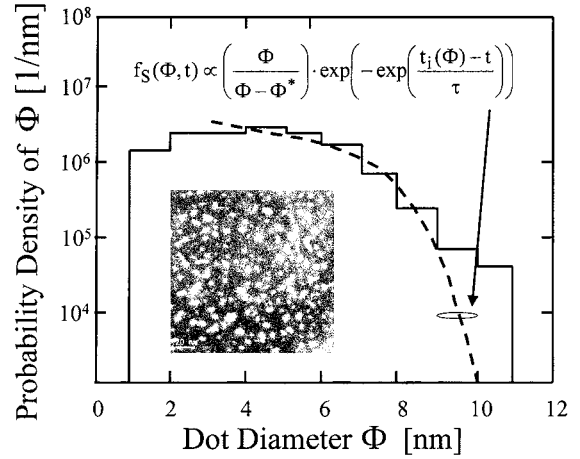


Fig. 3. Dot diameter experimental distribution coming from the energy filtered TEM image of LPCVD Si-dots (inset) and theoretical fitting (dashed line) based on a Shneidman solution of the Frenkel-Zeldovich [7] ($\Phi^* \approx 0$ is the critical diameter, $t_i(\Phi)$ is the incubation time, τ is the transient time, mean dot diameter $\sim 4.9 \text{ nm}$).

proportional to $\Delta g_s^* i^{2/3}$. The presence of a surface energy for the newly formed cluster produces a free energy barrier for the nucleation ΔG^* at a critical size i^* and the cluster free energy will produce a tendency to growth or shrinkage depending on whether $i > i^*$ or $i < i^*$. Assuming this driving force, the nucleation can be modeled by considering the balance equation of Frenkel-Zeldovich. Recently an analytical solution to this equation, for $i \gg i^*$ has been proposed by Shneidman for a number of different nuclei growth kinetics [7]. For a growth regime limited by the reaction rate at the surface, the Shneidman solution is

$$P_S(\Phi, t) \propto \frac{\Phi}{\Phi - \Phi^*} \cdot \exp\left(-\exp\left(\frac{t_j(\Phi) - t}{\tau}\right)\right) \cdot d\Phi. \quad (3)$$

In (3), Φ^* is the critical diameter corresponding to the critical size i^* , t is the deposition time, while t_j is another characteristic time function of dot diameter (i.e., incubation time).

Note that contrary to the previous case, this dot diameter model states that going to smaller Φ values, dot size probability remains constant. Indeed, the results provided by the Shneidman assumption for dot diameter distributions can be regarded as complementary to the Maxwell-Boltzmann case.

C. Total Number of Dots in a Cell: N_{td}

Concerning the total dot number in a cell N_{td} , we make the hypothesis that it is described by a Poisson law $P_{N_{\text{td}}}(\lambda)$, with $\lambda = \overline{N_{\text{td}}} = A \times D_{\text{dot}}$, D_{dot} being the dot areal density and A the cell area. This assumption derives from the fact that these statistics describes the behavior of random, rare events in space or time: random events, in space, because the nucleation of one dot does not influence the nucleation of another dot in the cell, and rare events, in space, because we do not consider cells where coalescence between dots shows up.

III. ANALYTICAL FORMULA OF MEMORY PROGRAMMING WINDOW ΔV_{th}

In a previous experimental and theoretical works [2], [8], [9], it has been demonstrated that the maximum programming

threshold voltage shift ΔV_{th} of one memory cell is proportional to the memory active area covered by the dots, R_{dot} , i.e.,

$$\begin{cases} \frac{dQ_{FG}}{dt} = J_1 - J_2 \\ \Delta V_{th} = R_{dot} \cdot \frac{Q_{FG}}{C_2}; R_{dot} = \frac{N_{td}}{A} \cdot \frac{\pi}{4} \cdot \overline{\Phi^2}; C_2 = \frac{\epsilon}{t_2} \end{cases} \quad (4)$$

where j_1 is the current density charging every Si-dot (coming from control gate and active canal), while j_2 is the current density discharging the Si-dots (going to control gate and active canal), both expressed in $[A/cm^2]$. C_2 is the control oxide capacitance per unit area $[F/cm^2]$, Q_{FG} is the local aerial density of charge supposed to be in each nanocrystal $[C/cm^2]$, t_1 is the tunnel oxide thickness, t_2 is the control oxide thickness.

As it can be deduced from this formula, the nanocrystal trapped charge is therefore considered as uniformly distributed all over the memory channel, as also reported by other authors [12], for evaluating its impact on the MOSFET operations.

If only the fluctuations of technological parameters of the Si-dots, as the dot size Φ and dot number N_{td} , are taken into account, it can be shown that $\sigma \Delta V_{th} \propto \sigma R_{dot}$, while (Q_{FG}/C_2) remains constant. Our attention, therefore, will be primarily focused on dot surface coverage ratio fluctuation. Note also that, as a confirmation of R_{dot} hypothesis, Ishii *et al.* [9] found experimentally that the mean programming window and its relative dispersion depends on dot surface coverage ratio, and not only on dot density.

Finally, it should be stated that in this model we have not taken into account coulomb blockade or quantum effects in the Si-dots. This assumption is coherent with our experimental results. In fact, our devices are based on Si nanocrystals highly dispersed in diameter ($>30\%$) and with dot diameter higher than 3–4 nm [10]. Moreover, consider that further improvements of our model should also take into account the electrostatic impact of dot position on the channel, to be consistent with memory devices with very narrow active channels (<30 nm) [11].

IV. MODELING OF THE PROGRAMMING WINDOW DISTRIBUTION

A. Monte Carlo Approach

First, a Monte Carlo (MC) simulation has been performed. The total number of dots for each cell is extracted, according to the Poissonian law. Then, in an independent way, for each dot in the cell, a different diameter is extracted, according to the chosen experimental law for dot diameter. The following expression is valid for the m th sample in the analyzed ensemble:

$$\Delta V_{th} = \frac{\pi \cdot Q_{FG}}{4A \cdot C_2} \cdot \sum_{i=1}^{N_{td,m}} (\Phi_i^2). \quad (5)$$

B. Compound Distribution Theory

1) *Analytical Exact Result of ΔV_{th} Distribution: CD Model:* From (5), it clearly appears that ΔV_{th} is a random sum (i.e., N_{td} depend on the cell) of random variables (i.e., Φ over the same cell, depends on the dot). This statistical process could be treated by means of the *Compound Distributions (CD) theory* [6].

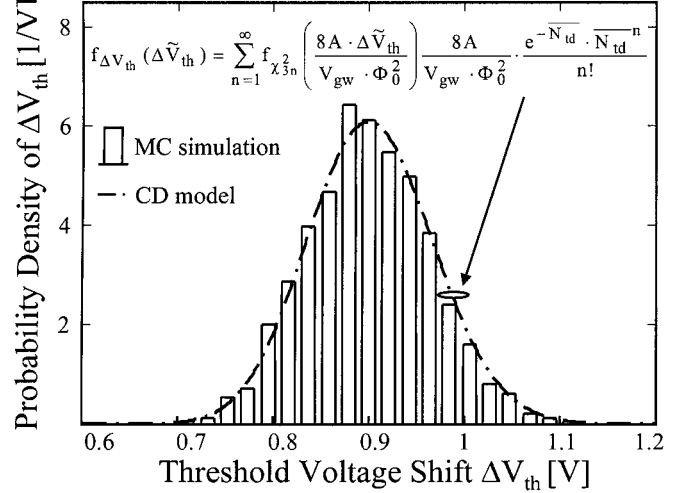


Fig. 4. Simulation of the ΔV_{th} histogram obtained with the MC method ((5), using 2000 samples). The theoretical probability based on the CD model (7) is also shown (parameters for simulation are: $A = 1.5 \times 10^{-10}$ cm², $D_{dot} = 2.1 \times 10^{12}$ cm⁻², $\Phi_0 = 2.7$ nm, $Q_{FG}/C_2 = 5$ V, $f_{\chi^2_{3n}}$ is a chi-squared distribution function with $3n$ degrees of freedom).

Indeed, this powerful theory allows us to give a complete description of the probability distribution $P_{\Delta V_{th}}$ of the programming window

$$\begin{aligned} P_{\Delta V_{th}}(\Delta \tilde{V}_{th}, \Delta \tilde{V}_{th} + d\Delta V_{th}) \\ = \sum_{n=1}^{\infty} P_{\Delta V_{th}}(\Delta \tilde{V}_{th}, \Delta \tilde{V}_{th} + d\Delta V_{th} | N_{td} = n) \\ \cdot P_{N_{td}}(N_{td} = n) \end{aligned} \quad (6)$$

where $P_{\Delta V_{th}}(\dots | N_{td} = n)$ is the ΔV_{th} probability conditioned to a number of dots per cell equal to n . In the case of the dot diameter experimental distribution like the Maxwell–Boltzmann one [(1), Fig. 2], the *exact* calculation of $P_{\Delta V_{th}}$ is feasible and the final analytical formula of the probability density $f_{\Delta V_{th}}$ is

$$\begin{aligned} f_{\Delta V_{th}}(\Delta \tilde{V}_{th}) = \sum_{n=1}^{\infty} f_{\chi^2_{3n}} \left(\frac{8A \cdot \Delta \tilde{V}_{th}}{\frac{Q_{FG}}{C_2} \cdot \pi \Phi_0^2} \right) \frac{8A}{\frac{Q_{FG}}{C_2} \cdot \pi \Phi_0^2} \\ \cdot \frac{e^{-N_{td}} \cdot N_{td}^n}{n!} \end{aligned} \quad (7)$$

where the role of the conditioned probability of (6) is played by a chi-squared function of $3 \cdot n$ degrees of freedom. To find out the result in (7), the result of (2) and an additional theorem on chi-squared distribution function has been used (i.e., $\chi_h^2 + \chi_m^2 = \chi_{h+m}^2$ [6]). In Fig. 4, a comparison between the CD and the MC models is provided.

2) *Analytical Approximated Result of ΔV_{th} Distribution: CD + CLT (Compound Distributions+Central Limit Theorem) Model:* In the case of not handy mathematical function for dot diameter distributions, as in the Shneidman assumption, an approximation could be employed, at least in the limit of a “large” number of dots on cells.

In (6), we mentioned already the presence of $P_{\Delta V_{th}}(\dots | N_{td} = n)$ as conditioned probability to the number of dots equal to n . In the case that n is rather high (i.e., more than 30) we know that the probability density in (6) approaches

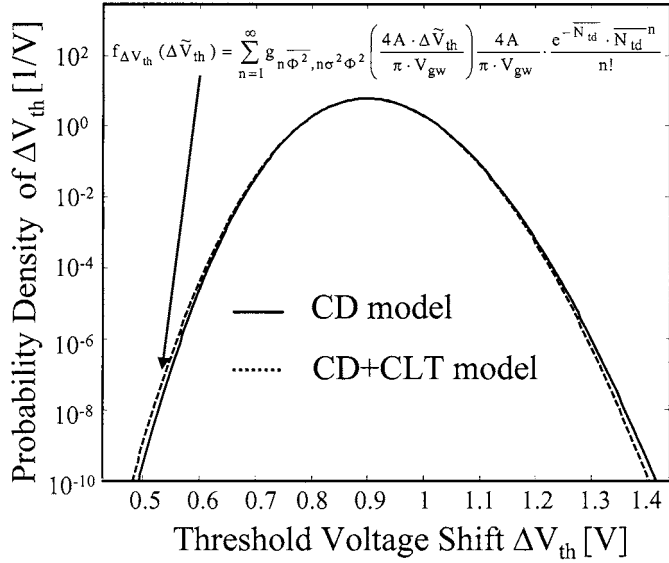


Fig. 5. Comparison between ΔV_{th} probability distribution obtained by means of the exact CD model (7), with same parameters as Fig. 4) and of the approximated CD + CLT model (8).

a sum of gauss distribution $g_{\mu, \sigma^2}(n^* \Phi^2)$ with mean value $\mu = n^* \bar{\Phi}^2$ and variance $\sigma^2 = n^* \sigma^2 \bar{\Phi}^2$, (6) becomes

$$f_{\Delta V_{th}}(\Delta \tilde{V}_{th}) = \sum_{n=1}^{\infty} g_{n, \bar{\Phi}^2, n \sigma^2 \bar{\Phi}^2} \left(\frac{4A \cdot \Delta \tilde{V}_{th}}{\pi \cdot \frac{Q_{FG}}{C_2}} \right) \frac{4A}{\pi \cdot \frac{Q_{FG}}{C_2}} \cdot \frac{e^{-\bar{N}_{td}} \cdot \bar{N}_{td}^n}{n!}. \quad (8)$$

In this case, the analytical result of $f_{\Delta V_{th}}$ is approximated. In Fig. 5, a comparison between the exact (CD model based) ΔV_{th} probability and the approximated one (CD + CLT model) is shown. The excellent agreement between the two approaches appears at least for probabilities higher than 10^{-10} .

3) *Numerical Result of ΔV_{th} Distribution:* Again in the case of not handy mathematical functions for dot diameter distributions, a *numerical result* on the programming window distribution could be provided. This method pushes the limit of the previous analysis to whatever value of dot number on cells.

In this case the conditioned probability $P_{\Delta V_{th}}(\dots | N_{td} = n)$ in (6) is calculated via a numerical convolution of n dot diameter distribution. Due to its numerical nature, this calculation starts directly from dot diameter histograms, without the need of an analytical fit (as in the Maxwell-Boltzmann or Shneidman case). In Fig. 6, a comparison between the programming window distribution starting from the Maxwell-Boltzmann assumption and the Shneidman assumption (both initially discretised) is provided, for a “low” number of dots on cells.

We see that the programming window distributions are similar to each other: starting from the Shneidman assumption, does not lead to substantially different result with respect to the Maxwell-Boltzmann case.

4) *Direct Calculation of $\overline{\Delta V_{th}}$ Mean Value and $\sigma \Delta V_{th} / \overline{\Delta V_{th}}$ Relative Standard Deviation:* Whenever the overall distribution expressions for N_{td} and Φ are not known, the CD theory also allows us to directly quantify the mean value ($\overline{\Delta V_{th}}$) and the relative variance ($\sigma \Delta V_{th} / \overline{\Delta V_{th}}$)

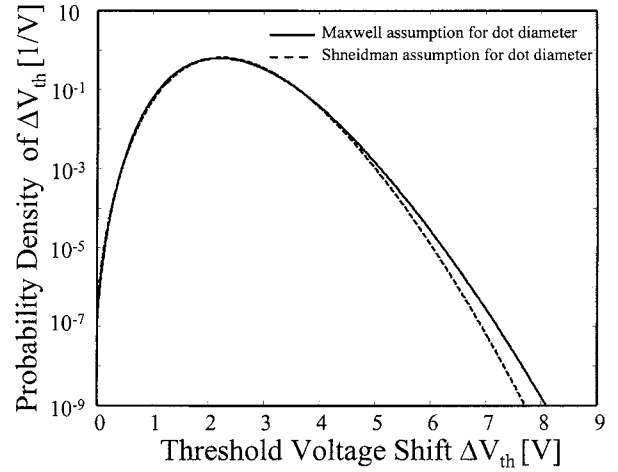


Fig. 6. Threshold voltage distributions starting from the Maxwell-Boltzmann assumption (solid line) or the Shneidman theory (dashed line) for dot diameter. This plot is the result of the numerical convolution of 21 Maxwell-Boltzmann or Shneidman simple probability densities, as $\bar{N}_{td} = 21$ ($A = 1 \times 10^{-11} \text{ cm}^2$, $D_{dot} = 2.1 \times 10^{12} \text{ cm}^{-2}$, $Q_{FG}/C_2 = 5 \text{ V}$). The mean value of dot diameter is $\sim 4.9 \text{ nm}$ for both distributions (the Shneidman distribution used is the same as Fig. 3, while $\Phi_0 = 4.35 \text{ nm}$ for Maxwell-Boltzmann distribution). We can see that, even for a low number of dots on cells, the programming window distributions do not differ much from each other.

of the programming window, starting from the equivalent parameters for N_{td} and Φ , i.e.,

$$\overline{\Delta V_{th}} = \frac{\bar{N}_{td}}{A} \cdot \frac{\pi}{4} \bar{\Phi}^2 \cdot \frac{Q_{FG}}{C_2} \quad (9)$$

$$\frac{\sigma^2 \Delta V_{th}}{\overline{\Delta V_{th}}^2} = \frac{\sigma^2 N_{td}}{\bar{N}_{td}^2} + \frac{1}{\bar{N}_{td}} \cdot \frac{\sigma^2 \Phi^2}{\bar{\Phi}^2}. \quad (10)$$

If the Poisson law is assumed for dot number on cell, (10) becomes

$$\frac{\sigma^2 \Delta V_{th}}{\overline{\Delta V_{th}}^2} = \frac{1}{\bar{N}_{td}} \cdot \left(1 + \frac{\sigma^2 \Phi^2}{\bar{\Phi}^2} \right). \quad (11)$$

Note that (9) and (10) simply quantify the separate influence of N_{td} and Φ characteristics on mean value and standard deviation of ΔV_{th} , feature hardly accessible with the MC model.

It is worthwhile to note that Ishii *et al.* [9] found experimentally that the relative variance of ΔV_{th} is equal to the relative variance of R_{dot} .

$$\frac{\sigma^2 \Delta V_{th}}{\overline{\Delta V_{th}}^2} = \frac{\sigma^2 R_{dot}}{\bar{R}_{dot}^2}. \quad (12)$$

This can be easily demonstrated, with the help of the CD theory, rewriting (10) for R_{dot} .

Another feature is that in the Maxwell-Boltzmann case (1) $\sigma^2 \Phi^2 / \bar{\Phi}^2 = 2/3$, whatever value of Φ_0 is considered, while in the Shneidman case $\sigma^2 \Phi^2 / \bar{\Phi}^2$ depends on the parameters considered.

V. DISCUSSION AND EXTRAPOLATIONS

A. Comparison Between Monte Carlo and Compound Distribution Model

Fig. 7 shows a comparison between the MC result and CD model concerning the value of $\sigma \Delta V_{th} / \overline{\Delta V_{th}}$. Note that the

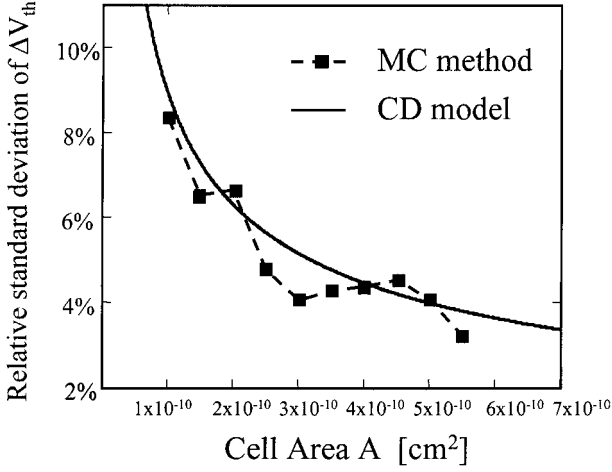


Fig. 7. Simulations of the relative standard deviation of ΔV_{th} versus the cell area A of memory cells. MC simulations (5) have been performed assuming 50 samples for each cell area. The Compound Distribution solid curve is based on (11) (assuming $D_{dot} = 2.1 \times 10^{12} \text{ cm}^{-2}$ and $\sigma^2 \Phi^2 / \bar{\Phi}^2 = 2/3$).

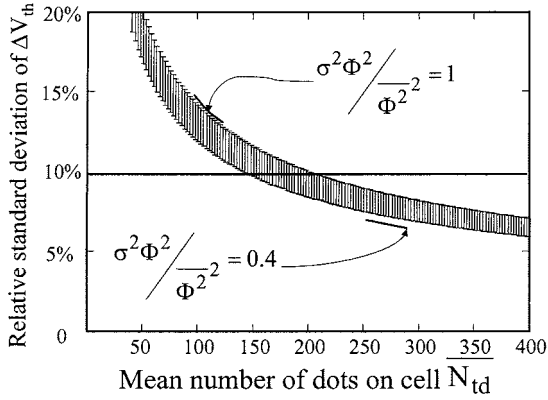


Fig. 8. Relative standard deviation of ΔV_{th} , as obtained from CD model (11). Two values of relative variance of dot size Φ^2 are shown. In order to obtain $\sigma \Delta V_{th} / \Delta V_{th} = 10\%$, it must be assured $\bar{N}_{td} > 140$, whatever combination of dot density or cell area is.

small discrepancies appearing between the two models are due to the fact that the MC method simulates results on a finite statistical ensemble of cells (50 samples in Fig. 7), while the CD model provides a theoretical result in the case of an infinite ensemble. Obviously, going to smaller cell areas the fluctuations of the MC simulations around the theoretical curve will become bigger and bigger, except if a larger number of cells is used for simulation.

In Fig. 8, a plot of the relative standard deviation of ΔV_{th} versus the mean number of dots per cell \bar{N}_{td} is provided. If a reliability criterion of $\sigma \Delta V_{th} / \Delta V_{th} < 10\%$ is imposed, in order to maintain a clear separation between the “1” and “0” memory programmed states, we have to assure a certain range of \bar{N}_{td} values (> 140) on our devices, for whatever combination of cell area and dot density. This means that going toward smaller and smaller cell areas, higher and higher dot density will be needed, which assures both small dispersion (10) and clearly detached memory states (9).

From (11), we can easily quantify the impact of dot number or dot diameter fluctuations separately considered. It could be interesting, for instance to quantify the influence of dot size

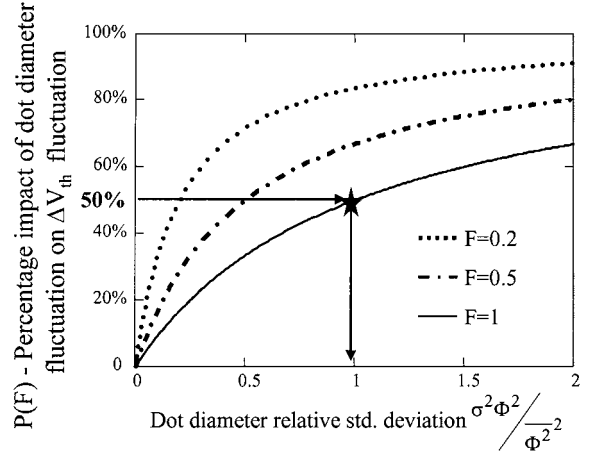


Fig. 9. Percentage impact of the relative dispersion of dot diameter on the overall programming window dispersion, $P(F)$, versus the relative dispersion of the dot diameter $\sigma^2 \Phi^2 / \bar{\Phi}^2$ [as coming from (13)]. The dot number relative variance assumes three values ($F = 1$ means Poisson distribution, $F = 0.2$ and $F = 0.5$ show possible future dot depositions toward “ordered” structures). We see that, while lowering $P(F)$, thus diminishing dot number fluctuation, dot size fluctuation plays a stronger and stronger role on $\sigma \Delta V_{th} / \Delta V_{th}$. For a dot number distribution equal to the Poisson law, it is highlighted the value of $\sigma^2 \Phi^2 / \bar{\Phi}^2$ which impacts at same percentage of $\sigma^2 N_{td} / \bar{N}_{td}^2$.

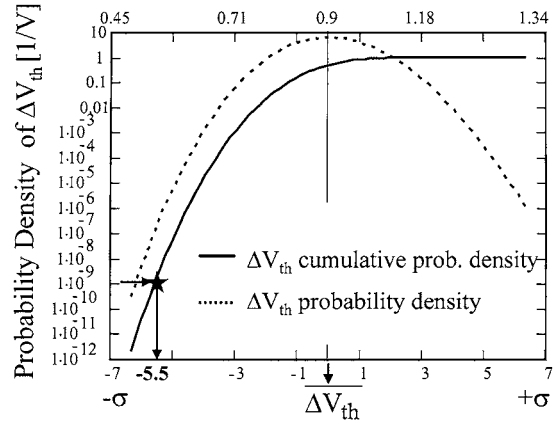


Fig. 10. Threshold voltage shift cumulative probability density (solid line) and probability density (dashed line) for the same parameters as in Fig. 4. The cumulative probability distribution is important to quantify the number of cells which show a threshold voltage shift below a certain limit (quantify the erratic bits). As an example, it is highlighted the voltage limit shown by one cell over a gigabit array.

fluctuation on the programming window dispersion, by letting $\sigma^2 \Phi^2 / \bar{\Phi}^2$ vary and calculate its impact on $\sigma \Delta V_{th} / \Delta V_{th}$. Concerning dot number, different distributions from the Poisson one could be also considered. To this aim a parameter F is introduced, where $F = 1$ stands for the Poisson dispersion. If $F < 1$ the dot number dispersion is less than the Poisson dispersion. We could imagine that the lower is the value of F , the higher is the order of dots deposited on the cell surface. We could now introduce a function $P(F)$ which quantifies the percentage impact of the term associated to the dot size fluctuation on the overall ΔV_{th} relative fluctuation. Eventually $P(F)$ is defined as follows:

$$P(F) = \frac{\frac{1}{A \cdot D_{dot}} \cdot \frac{\sigma^2 \Phi^2}{\bar{\Phi}^2}}{\frac{F}{A \cdot D_{dot}} + \frac{1}{A \cdot D_{dot}} \cdot \frac{\sigma^2 \Phi^2}{\bar{\Phi}^2}} \quad (13)$$

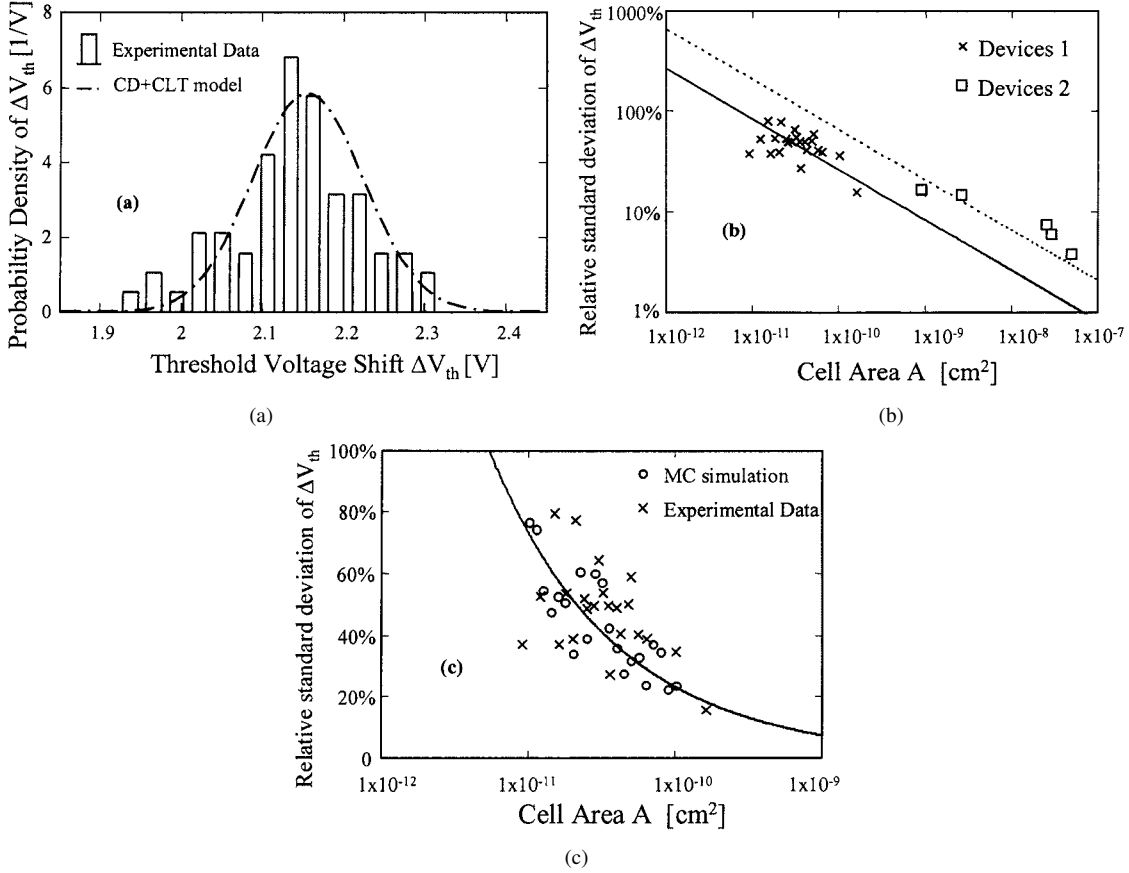


Fig. 11. (a) Comparison between experimental data of Device 1 ($W = 10 \mu\text{m}$, $L = 0.5 \mu\text{m}$) and CD+CLT model (8), using this set of parameters (1): $\bar{\Phi} = 7 \text{ nm}$, $\sigma^2\Phi^2/\bar{\Phi}^2 = 0.6$, $D_{\text{dot}} = 1 \times 10^{11}/\text{cm}^2$ with $\sim 1/4$ of dots effectively charged). (b) Relative standard deviation of ΔV_{th} versus cell area. Experimental results are evidenced by crosses (Device 1) and boxes (Device 2). Fits using the CD model (11) have been done using parameter set (1) for Device 2 and parameter set (2) (i.e., $\sigma^2\Phi^2/\bar{\Phi}^2 = 1$, $D_{\text{dot}} = 1 \times 10^{12}/\text{cm}^2$ with $\sim 1/4$ of dots effectively charged) for Device 1. (c) Comparison between data of Device 1, CD model (11) with parameter set (2) and MC simulations [circles, (5)] using 20 samples per area, to simulate a real dispersion (due to a limited statistical ensemble) around the theoretical curve.

In Fig. 9, the result of (13) is shown for three different values of F . The CVD deposition method assures, at the moment, a typical Poisson dot number fluctuation (i.e., $F = 1$), therefore it is highlighted on its curve that $\sigma^2\Phi^2/\bar{\Phi}^2 = 1$ impacts for 50% on $\sigma\Delta V_{\text{th}}/\overline{\Delta V_{\text{th}}}$. Most of the techniques used nowadays for Si-dot deposition assure typical values of $\sigma^2\Phi^2/\bar{\Phi}^2$, between 0.4 and 1. In this case the most important contribution to programming window dispersion is due to dot number fluctuation.

B. Erratic Bits

It is possible to quantify the number of cells under a certain limit of surface coverage ratio, i.e., the cells in an array which will not show a sufficient programming window. These cells, could be called *erratic bits* in the case of multi nanocrystal memories.

To know the amount of erratic cells, the cumulative probability density $F_{\Delta V_{\text{th}}}$ of the programming window must be computed, thus, if we start, for instance, from the result of CD model (7), we obtain

$$F_{\Delta V_{\text{th}}}(\Delta\tilde{V}_{\text{th}}) = \sum_{n=1}^{\infty} F_{\chi_{3n}^2} \left(\frac{8A \cdot \Delta\tilde{V}_{\text{th}}}{\frac{Q_{\text{FG}}}{C_2} \cdot \pi\Phi_0^2} \right) \cdot \frac{e^{-\overline{N_{\text{td}}} \cdot \overline{N_{\text{td}}}^n}}{n!} \quad (14)$$

where $F_{\chi_{3n}^2}$ is the cumulative probability function of χ_{3n}^2 . As an example, in Fig. 10 the cumulative probability distribution is shown, as coming from (14) and same parameters used for Fig. 4 or Fig. 5. It is highlighted the ΔV_{th} value which is at most supposed to be shown by one cell in a gigabit array (probability of 10^{-9}). It is worthwhile to remark that (13) shows the diverse dependences, i.e., Φ_0 , N_{td} , A , Q_{FG}/C_2 , which could be arranged to suit one's reliability requirements.

Following the previous reasoning, a simple formula to quantify the erratic bits with the CD+CLT model could be provided, as well. In this case $F_{\Delta V_{\text{th}}}$ is a sum of G_{μ, σ^2} error functions

$$F_{\Delta V_{\text{th}}}(\Delta\tilde{V}_{\text{th}}) = \sum_{n=1}^{\infty} G_{n, \overline{\Phi}^2, n \cdot \sigma^2\Phi^2} \left(\frac{4A \cdot \Delta\tilde{V}_{\text{th}}}{\pi \cdot \frac{Q_{\text{FG}}}{C_2}} \right) \cdot \frac{e^{-\overline{N_{\text{td}}} \cdot \overline{N_{\text{td}}}^n}}{n!} \quad (15)$$

VI. COMPARISON WITH EXPERIMENTAL DATA

In Fig. 11, *experimental evidence* of the validity of the CD model is given. Two different types of devices with several active areas have been fabricated and tested.

Device 2 corresponds to Si-bulk memory transistors [8], defined by ultraviolet lithography, with minimum area of $W \times L = 0.35 \times 0.25 \mu\text{m}^2$ and maximum area of $W \times L = 10 \times$

0.5 μm^2 . In Device 2, the total dot number is on the order of thousands ($D_{\text{dot}} \approx 1 \times 10^{11} \text{ cm}^{-2}$). Device 1 corresponds to a silicon-on-insulator memory transistor [12], defined by e-beam lithography, with minimum area of $W \times L = 30 \times 40 \text{ nm}^2$ and maximum area of $W \times L = 80 \times 200 \text{ nm}^2$. In Device 1, the total dot number is on the order of tens ($D_{\text{dot}} \approx 1 \times 10^{12} \text{ cm}^{-2}$). Silicon dots in large area cell (Device 2) were LPCVD deposited with a low areal density, while silicon dots in nanoscaled cells (Device 1) were fabricated via annealing of LPCVD SiO_x enriched layer. This last fabrication method of dots is believed to develop islands with a high areal density but largely dispersed in size. Both types of devices have been written and erased in fully Fowler–Nordheim conditions. Each cell corresponds to a different chip on the 8'' wafers.

Systematic tests were carried out on an ensemble of ~ 50 cells, in the case of large devices, while on an ensemble of ~ 20 devices in the case of nanoscaled devices. In Fig. 11(a), in particular, the comparison between the CD + CLT model (8) and experimental results is provided, in the case of Device 2. In Fig. 11(b), (11) has been applied considering around one fourth of dots effectively charged, and $\sigma^2\Phi^2/\overline{\Phi}^2 = 0.6$ in the case of Device 2, while $\sigma^2\Phi^2/\overline{\Phi}^2 = 1$ in the case of Device 1.

In Fig. 11(c) is evidenced also the MC simulation on nanoscaled cells. The spread around the theoretical curve is due to the small number of samples considered (in simulations 20 samples per cell area are taken, as in the experimental data).

VII. CONCLUSIONS

A detailed model, tailored on multinanocrystal memory devices, on programming window dispersion has been provided. Both a Monte Carlo simulation and a theoretical approach based on the compound distributions theory have been introduced to fix quantitatively guidelines concerning dot density and dot size requirements. The separated impact of dots diameter or dots number fluctuations on the overall dispersion, $\sigma\Delta V_{\text{th}}/\Delta V_{\text{th}}$, has also been quantified. The main issue of erratic bits (i.e., cells with too low programming window) in an ensemble of multinanocrystal memories has been addressed as well.

The validity of our approach has been confirmed by the very good agreement between our simulations and a large set of experimental data.

ACKNOWLEDGMENT

The authors thank G. Molas from CEA-LETI and L. Baldi from STMicroelectronics for helpful discussions.

REFERENCES

- [1] J. DeBlauwe, "Nanocrystal nonvolatile memory devices," *IEEE Trans. Nanotechnol.*, vol. 1, p. 72, Mar. 2002.
- [2] C. M. Compagnoni, A. Spinelli, A. Lacaita, and C. Gerardi, "Study of nanocrystal memory reliability by CAST structures," in *Proc. Int. Reliability Physics Symp.*, 2003.
- [3] S. Lombardo, C. Gerardi, D. Corso, G. Ammendola, I. Crupi, and M. Melanotte, "Effects of the distributed charge storage in nanocrystal memory cell," in *Proc. Nonvolatile Semiconductor Workshop*, 2003, p. 105.

- [4] D. Burnett, J. Higman, A. Hoefler, C. B. Li, and P. Kuhn, "Variation in natural threshold voltage of NVM circuits due to dopant fluctuations and its impact on reliability," in *Int. Electronic Device Meeting Tech. Dig. (IEDM)*, 2002, p. 529.
- [5] F. Mazen, T. Baron, G. Brémond, N. Buffet, N. Rochat, P. Mur, and M. N. Séméria, "Influence of chemical properties of the substrate on silicon quantum dot nucleation," *J. Electrochem. Soc.*, vol. 150, pp. G203–G208, 2003.
- [6] W. Feller, *An Introduction to Probability Theory and its Applications*. New York: Wiley, 1968, ch. XII.
- [7] V. A. Shneidman, "Size distribution of new-phase particles during transient condensation of a supercooled gas," *Sov. Phys. Tech. Phys.*, vol. 33, p. 1338, 1988.
- [8] B. De Salvo, G. Ghibaudo, G. Pananakakis, P. Masson, T. Baron, N. Buffet, A. Fernandes, and B. Guillaumot, "Experimental and theoretical investigation of nano-crystal and nitride-trap memory devices," *IEEE Trans. Electron Devices*, vol. 48, pp. 1789–1798, Aug. 2001.
- [9] T. Ishii, T. Osabe, T. Mine, F. Murai, and K. Yano, "Engineering variations: toward practical single-electron (few-electron) memory," in *Int. Electron Device Meeting (IEDM) Tech. Dig.*, 2000, pp. 305–308.
- [10] H. Wang, N. Takahashi, H. Majima, T. Nukai, M. Saitoh, and T. Hiramoto, "Effects of dot size and its distribution on electron number control in metal-oxide-semiconductor field-effect-transistor memories based on silicon nanocrystal floating gate," *Jpn. J. Appl. Phys.*, vol. 40, pp. 2038–2040, 2001.
- [11] M. Saitoh, E. Nagata, and T. Hiramoto, "Effects of ultra-narrow channel on characteristics of MOSFET memory with silicon nanocrystal floating gate," in *Int. Electron Device Meeting (IEDM) Tech. Dig.*, 2002, pp. 181–184.
- [12] T. Molas, B. De Salvo, G. Ghibaudo, D. Mariolle, N. Buffet, S. Lombardo, and S. Deleonibus, "Investigation of few electron storage phenomena in an ultrascaled Si-nanocrystal memory," in *Proc. Silicon Nanoelectric Workshop (SNW)*, 2003.
- [13] L. Guo *et al.*, "Fabrication and characterization of room temperature silicon single electron memory," *J. Vac. Sci. Technol. B*, vol. 15, no. 6, Nov./Dec. 1997.